Transmission/reflection analysis for distributed optical fibre loss sensor interrogation

V.V. Spirin, M.G. Shlyagin, S.V. Miridonov and P.L. Swart

A novel interrogation method for fibre optic loss sensors based on the analysis of transmitted and reflected powers of a continuous wave light source is presented. The position of the loss region is determined from unique dependencies between normalised powers for different locations of the disturbance along the fibre containing a number of Bragg gratings.

Introduction: Distributed fibre optic sensors based on bend-induced excess losses are very attractive for the measurement of pressure, temperature, displacement, etc. where the measurand can be associated with a lateral deformation of the fibre [1, 2]. The fibre section where additional light losses occur can be localised by means of optical time-domain reflectometry (OTDR) [3] or frequency domain reflectometry, such as coherent (COFDR) [4] and incoherent optical frequency domain reflectometry (IOFDR) [5, 6]. In this Letter, we present what is to our knowledge the first transmission/reflection analysis (TRA) for detection and localisation of excess bending losses using an unmodulated continuous-wave (CW) light source.

Experiment: The experimental setup for verification of the TRA method is shown in Fig. 1. The light emitted from a super-luminescent diode operating at a central wavelength of 1550 nm with a linewidth of about 50 nm was launched into a singlemode test fibre through an optical circulator. The launched optical power was about 400 μW. The optical isolator was used to prevent back reflection from the output end of the test fibre. A standard two-channel lightwave multimeter was used to measure the transmitted and reflected power from the test fibre. The sensing fibre comprises four segments L_1–L_4 with bending transducers (BT) (see Fig. 1) for inducing the excess bending losses, separated by three Bragg gratings BG_1–BG_3. In our experiment, the distances between neighbouring gratings were chosen to be about 25 cm. However, these distances are limited only by internal losses in the test fibre and can be up to a few kilometres. The Bragg gratings were written in the core of the singlemode fibre by using a phase mask technique and a pulsed excimer laser operating at a wavelength of 248 nm. The gratings had equal lengths of 1.5 mm each, and maximum reflectivities equal to 4.2, 5.3 and 8.0% respectively.
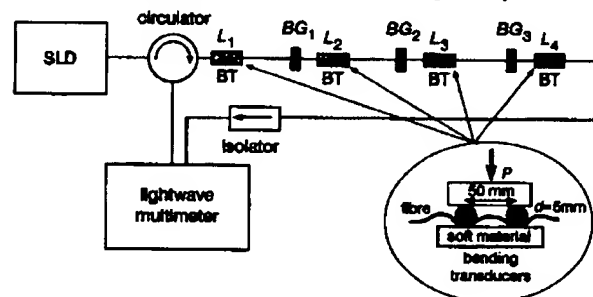

Fig. 1 *TRA sensor configuration*

As is well known, the measurement of excess loss in optical fibres can be used to determine the value of the perturbations that introduced this loss [1, 2]. The basic principle of the TRA method is to use the unique relationships between normalised transmitted and reflected powers of an unmodulated CW light source for different locations of the disturbance along the sensing fibre. Powers are normalised with respect to their initial undisturbed values. If, for example, the bending loss occurs at the last fibre segment L_4 (see Fig. 1), increasing the load P leads to a proportional decrease in the transmitted power. However, it does not change the reflected power. But if we bend the first fibre segment L_1, a decrease in transmitted power is accompanied by a decrease in the reflected power. In general, the value of the decrease in normalised power depends on the location of the perturbation (between two Bragg gratings). Fig. 2 shows calculated dependencies between normalised transmitted and reflected powers when additional bending losses occur at different fibre segments. To find this family of para-

metric curves, we used an algorithm that successively calculates the transmission and reflection of a series of mirrors and lossy fibre segments. The parameter here corresponds to the segment number where the perturbation is applied. The algorithm takes into account multiple reflections. The calculation was performed for the reflectivity of lumped reflectors corresponding to the maximum reflectivity of the Bragg gratings which was used in our experiment. Fig. 2 also presents the results of experimental measurements of normalised transmitted and reflected powers for additional bending losses that were induced at the different fibre segments. Small discrepancies between measured and calculated values are mainly due to the non-perfect suppression of reflections in connectors.
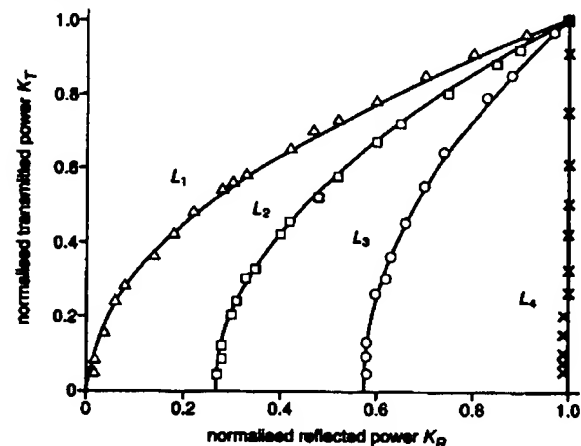

Fig. 2 *Theoretical and experimental relationship between normalised transmitted and reflected powers for excess losses induced at different fibre segments*

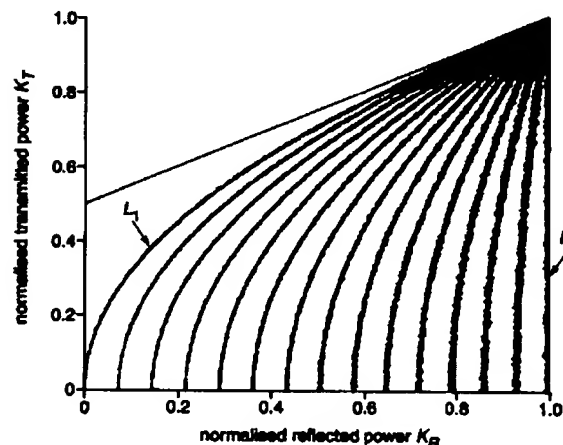—— theoretical curves

△, □, ○, × measured data

Fig. 3 *Calculated parametric curves for sensor comprising 15 sensing segments and 14 reflectors, each with a 0.1% reflectivity*

Note that the proposed TRA method can localise only a single perturbation that may appear along the sensing fibre. With this method, we can localise the perturbation with a spatial resolution that is determined by the distance between neighbouring lumped reflectors. To increase the resolution, we should increase the number of lumped reflectors while simultaneously reducing the individual reflectivities. Fig. 3 shows the result of the numerical calculation of 15 fibre segments separated by lumped reflectors with a reflectivity of 0.1% each. We modelled the effect of noise by introducing random fluctuations in a small excess loss term for each fibre segment. This loss was assumed to be uniformly distributed between 0 and 0.3%. For these parameters, the family of curves are approximately equi-distributed between the L_1 and the L_{15} curves. Therefore, to localise the perturbation for a normalised transmitted power of less than 0.1, we need to measure the normalised reflected power with an accuracy better than R_{max}/N, where R_{max} is the total reflected power from the undisturbed sensing fibre, and N is the

number of segments. For the localisation of a weaker perturbation where the slope of the left-most curve approaches 0.5 (upper right end in Fig. 3), the required accuracy should be $2(1 - K_T)(R_{max}/N)$, where K_T is the normalised transmitted power in the presence of a weak perturbation. For example, for 15 segments and for $K_T = 0.9$, we need to measure the normalised reflected power with an accuracy better than $R_{max}/45$ compared with $R_{max}/15$ for a strong perturbation. It is therefore easier to localise a strong perturbation with the TRA method. Another important feature of this method, which should be stressed, is that the noise level increases with the distance along the sensing fibre (see Fig. 3). However, this effect can be suppressed if we provide symmetrical measurements from the other end of the sensing fibre. Furthermore, the symmetrical configuration also allows for the localisation of two strong disturbances simultaneously.

Conclusion: We have demonstrated that the proposed TRA-based bending sensor allows for the localisation of one loss-inducing perturbation along a sensing fibre by measuring only transmitted and reflected powers of unmodulated CW light. As we believe, this technique should be very attractive for the eventual realisation of inexpensive distributed fibre optic sensors.

V.V. Spirin, M.G. Shlyagin and S.V. Miridonov (*Division de Física Aplicada, CICESE, Apdo. Postal No. 2732, CP 22860, Ensenada, B.C., México*)

E-mail: vaspir@cicese.mx

P.L. Swart (*EE Dept., Faculty of Engineering, Rand Afrikaans University, PO Box 524, Auckland Park 2006, Republic of South Africa*)

References

1 NOLAN, D.A., BLASZYK, P.E., and UDD, E.: 'Optical fibers' *in* 'Fiber optic sensors: an introduction for engineers & scientists' (John Wiley & Sons, New York, 1991)
2 MITCHELL, G.L.: 'Intensity-based and Fabry-Perot interferometer sensors' *in* 'Fiber optic sensors: an introduction for engineers & scientists' (John Wiley & Sons, New York, 1991)
3 TATEDA, M., and HORIGUCHI, T.: 'Advances in optical time domain reflectometry', *J. Lightwave Technol.*, 1989, 7, pp. 1217–1224
4 TSUJI, K., SHIMIZU, K., HORIGUCHI, T., and KOYAMADA, Y.: 'Coherent optical frequency domain reflectometry for a long single-mode optical fiber using a coherent lightwave source and an external phase modulator', *IEEE Photonics Technol. Lett.*, 1995, 7, pp. 804–806
5 PIERCE, S.G., MACLEAN, A., and CULSHAW, B.: 'Optical frequency-domain reflectometry for microbend sensor demodulation', *Appl. Opt.*, 2000, 39, pp. 4569–4581
6 VENKATESH, S., and DOLFI, D.W.: 'Incoherent frequency modulated CW optical reflectometry with centimeter resolution', *Appl. Opt.*, 1990, 29, pp. 1323–1326

gets low (latching phase), the voltages at the two outputs start rising. After the output voltages reach a certain value (the switching threshold voltage of the comparator) the cross-coupled transistors M3 and M4 form a positive feedback and, depending upon the initial currents of M1 and M2, one of the outputs goes to V_{dd} and the other one goes to GND. When the two outputs reach their final values, they stay there until the Reset signal goes high again.
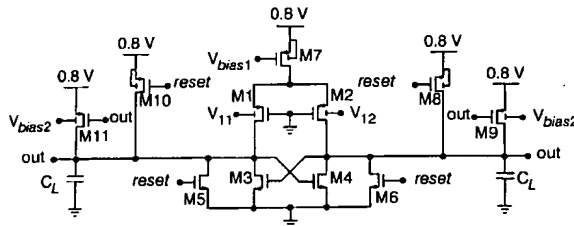

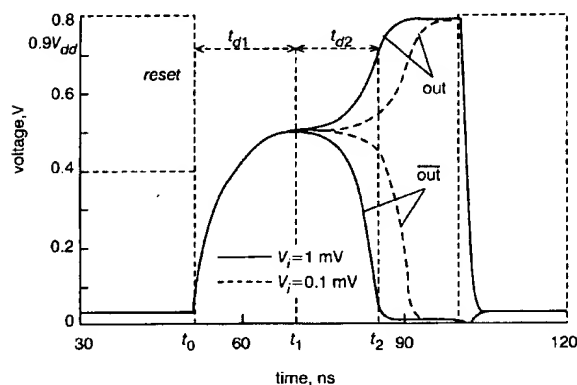Fig. 2 Schematic diagram of 1-bit quantiser

Fig. 3 Transient response of comparator for two different input levels

Fig. 3 shows the transient response of the comparator with a capacitive load of 1 pF running at a frequency of 10 MHz. The transient response depicts two cases: (i) $V_i = 1$ mV, and (ii) $V_i = 0.1$ mV. As can be seen when the input has a larger value, the comparator response is faster. This is because the difference between the currents of M1 and M2 is larger. This larger difference enables the quantiser to reach its switching threshold quickly. The delay response of the comparator in the latching phase can be divided into two time periods. In the first period, the two outputs take finite time to charge to the quantiser switching threshold (t_{d1}). During this time the positive feedback is not yet triggered. In the second period after the positive feedback is turned-on, it takes time t_{d2} to reach its final value. These two delay times (t_{d1} and t_{d2}) depend on the differential input voltage (V_i). Table 1 shows t_{d1}, t_{d2}, and the total delay ($t_d = t_{d1} + t_{d2}$) of the comparator for different differential values of V_i. As can be seen, the total delay of the comparator depends on the input voltage. Therefore, there is a compromise between the maximum operating frequency of the comparator and the input voltage resolution (how small the input can be). Post-layout simulation results show (Table 1) that when the differential input voltage is 10 μV, the delay of the comparator is 49.15 ns. This delay should be smaller than half period of the clock. Therefore, running the comparator at a clock frequency of 10 MHz can provide a resolution of 10 μV. Increasing the clock frequency to 12 MHz results in the lowering of the quantiser resolution to 100 μV. In the proposed circuit, transistors M8 to M11 are used to speed up the circuit. These transistors source currents to output nodes after the Reset is inactivated. This causes the outputs to rise faster and t_{d1} is reduced. The body of transistors M9 and M11 are biased to reduce their threshold voltage and get the most benefit of them in this low voltage circuit. It is also possible to increase the biasing current and size of the input transistors to reduce the delay. However, this will increase the power consumption of the circuit. Therefore, there is a compromise between speed and power consumption.

Table 1: Delay of comparator for different differential input values

V_i	10 μV	100 μV	1 mV	10 mV
t_{d1} (ns)	26.25	23.05	19.95	16.75
t_{d2} (ns)	22.90	19.20	15.80	12.30
t_d (ns)	49.15	42.25	35.75	29.05

Conclusion: A new comparator using the body of the PMOS transistors is proposed. This comparator can be used as a 1-bit quantiser in sub-1 V ΔΣ modulators. One of the main issues in the design of low voltage analogue circuits is the coupling of different blocks. The input of the proposed quantiser can vary between V_{dd} and GND. Therefore, the comparator can be directly connected to the preceding opamp in a ΔΣ modulator. The post-layout simulation results of the comparator, using BSIM3 model, are presented. We have successfully used this comparator in 0.8 V fully differential first-order and second-order ΔΣ modulators as a 1-bit quantiser. The clock frequency of these modulators is 10 MHz. The quantiser consumes a power of 134 μW. The circuit-level simulations show that, with an over sampling ratio of 200, the first-order and the second-order modulators achieve a maximum SNR of 72 and 93 dB, respectively.

References

1 PELUSO, V., VANCORENLAND, P., MARQUES, A.M., STEYAERT, M.S.J., and SANSEN, W.: 'A 900-mV low power ΔΣ A/D converter with 77-db dynamic range', IEEE J. Solid-State Circuits, 1998, 33, (12)

2 LEHMAN, T., and CASSIA, M.: '1-V power supply CMOS cascode amplifier', IEEE J. Solid-State Circuits, 2001, 36, (7)

3 MAYMANDI-NEJAD, M., and SACHDEV, M.: 'Continuous time common mode feedback technique for sub 1-V analogue circuits', Electron. Lett., 2002, 38, (23)

4 DESSOUKY, M., and KAISER, A.: 'Very low voltage digital audio ΔΣ modulator with 88-dB dynamic range using local switch bootstrapping', IEEE J. Solid-State Circuits, 2001, 36, (3)

Distributed fibre-optic loss sensor with chirped Bragg grating based on transmission-reflection analysis

V.V. Spirin, P.L. Swart, A.A. Chtcherbakov, S.V. Miridonov and M.G. Shlyagin

A novel distributed fibre-optic loss sensor with chirped Bragg grating based on the analysis of transmitted and reflected powers is presented. The localisation of loss region with error equal to ±2 mm along the 10 cm chirped grating for 0.7 dB induced loss is demonstrated.

Introduction: Distributed loss fibre-optic sensors are very attractive for the measurement of pressure, temperature, displacement, etc., where the measurand is associated with induced losses [1]. In our previous works we have reported a novel principle for localisation of a loss-inducing perturbation based on transmission-reflection analysis (TRA) using an unmodulated light source with a test fibre having several imprinted short Bragg gratings [2], or utilising the Rayleigh backscattering phenomenon [3, 4]. Localisation of a strong disturbance with a maximum localisation error of a few metres along a few km-long singlemode sensing fibre was demonstrated. However, for some applications it is important to localise even weak alarm-like perturbations with very high accuracy.

In this Letter we present a novel distributed fibre-optic sensor based on transmission-reflection analysis with a chirped fibre Bragg grating that allows one to pinpoint the lossy region with high accuracy.

Experimental setup and operating principle: The schematic diagram of the proposed TRA-based fibre-optic sensor is shown in Fig. 1. Continuous-wave light emitted by a superluminescent diode operating near 1550 nm wavelength with a line width of about 50 nm was launched through an optical circulator into a singlemode fibre containing the chirped Bragg grating. The launched optical power was about 0.33 mW. The optical isolator cancelled any back reflections from the output end of the test fibre. A dual-channel lightwave meter was used to measure the transmitted and Rayleigh backscattered powers. To induce the bending losses in the sensing fibre, we used bending transducers, which are also shown schematically in Fig. 1. The losses were induced by bending approximately 1–2 mm of chirped grating at different positions. By tuning the bending transducer, we could change the normalised transmitted power by more than −30 dB from its initial undisturbed value. Reflections from the source-end and the remote-end of the sensing fibre were equal to 1.5×10^{-5} and 2.0×10^{-5}, respectively.
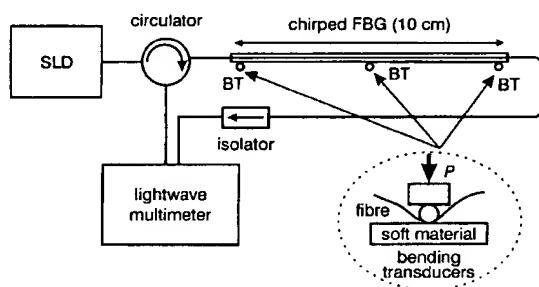

Fig. 1 *Distributed fibre-optic TRA sensor with chirped FBG*

The linearly chirped Bragg gratings were written in the core of the photosensitive singlemode fibre by using a 10 cm length phase mask and a pulsed excimer laser operating at a wavelength of 248 nm. The period of the linearly chirped Bragg grating varies linearly along the length of the grating. As a result, the different parts of the grating reflect different bands of wavelengths. Therefore, the total reflected power depends on the location of the loss region. If the bending losses occur at the remote-end of the grating (see Fig. 1), an increase in the loss leads to a proportional decrease of the transmitted power. However, it does not change the total reflected power. In contrast, if we bend the grating close to the source-end, the decrease of the transmitted power is accompanied by a decrease of the reflected power. In general, for identical loss-induced perturbations, the value of the decrease in normalised reflected power depends on the location of the excess loss region. Therefore, the localisation of the loss region can be performed by measurement of the transmitted and reflected powers.

Experimental results and discussion: Fig. 2 shows the relationships between normalised reflected power and the square of the normalised transmitted power for the excess loss induced at different positions along the grating. The relationships are approximately linear for a perturbation which may affect the test fibre at any location. The unique slopes of the lines depend on the position of the perturbation along the test fibre. Note that qualitatively the same linear dependencies were observed for the sensor utilising Rayleigh backscattering [4]. Hence, the localisation of the perturbation with the TRA method can be performed by evaluation of the slope of the line representing the dependence of normalised reflected power against the square of normalised transmitted power for the sensor comprising the linearly chirped Bragg grating.

The accuracy of localisation of excess loss with the TRA method strongly depends on the value of the induced loss. With the TRA method, it is easier to localise strong perturbations. The localisation of a weak perturbation requires higher measurement accuracy for the transmitted and Rayleigh backscattered powers. In contrast to this, the accuracy of localisation of loss with a standard optical time domain reflectometer depends mainly on the duration of the optical test pulse

and is practically independent on the value of the loss. We estimated the localisation error of the TRA method from the variations of reflected power for strong bending losses that decrease the fibre transmission by more than 30 dB. Fig. 3 shows the variations of normalised reflected power for strong losses induced near the remote-end of the test fibre for 20 min. The maximum deviation of normalised reflected power was approximately equal to $\pm 6 \times 10^{-3}$. This value allows us to estimate that the maximum localisation error should be equal to ± 0.5 mm for a strong perturbation at any location along the 10 cm-length of test fibre containing the grating. In practice, however, the accuracy of the localisation was worse. In addition to bending the optical fibre at a predetermined location, we introduced additional losses by arbitrary bending of other parts of the grating. This resulted in an extra localisation error. Another reason for the increased localisation error is related with an imperfection of the grating. However, this error can be efficiently compensated by means of an appropriate calibration procedure. Fig. 2 shows the relationships between the normalised reflected and the square of the normalised transmitted powers for the losses induced at three locations separated by 4 mm. Although these losses decreased the initial transmission by 15% only, the different locations of the perturbation can be clearly distinguished. The maximum localisation error estimated from the data presented in Fig. 2 is equal to ± 2 mm. Note that the length of the grating can be increased at least severalfold without loss of localisation accuracy.
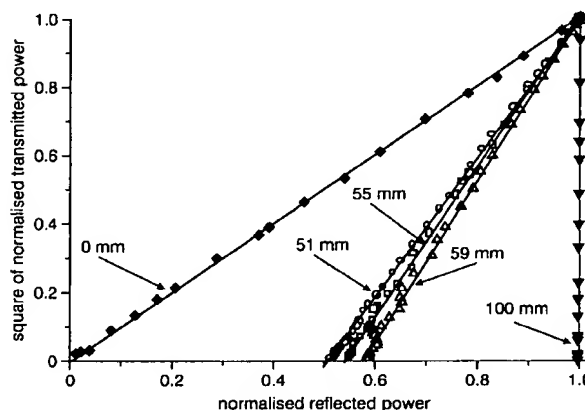

Fig. 2 *Functional dependence of normalised reflected and the square of normalised transmitted powers for losses induced at different positions along chirped grating*
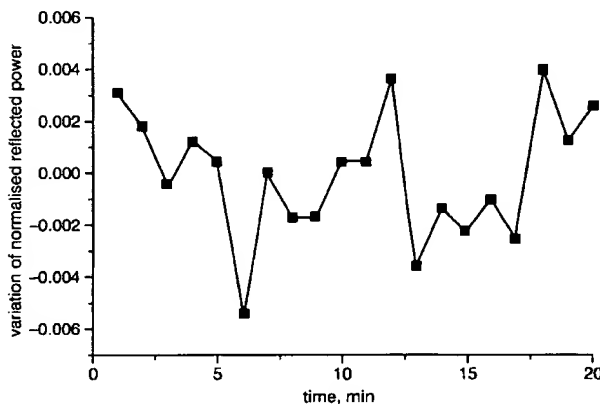

Fig. 3 *Variation of normalised reflected power for strong losses induced near remote-end of fibre*

Conclusion: We have demonstrated that a distributed fibre-optic sensor based on the TRA principle with a linearly chirped Bragg grating provides high localisation accuracy of the loss-induced perturbation. Localisation of both strong and weak bending disturbances with a maximum localisation error equal to ± 2 mm along 10 cm-length sensing fibre was demonstrated.

V.V. Spirin, S.V. Miridonov and M.G. Shlyagin (Division de Fisica Aplicada, CICESE, Apdo. Postal No. 2732, CP 22860, Ensenada, B.C., México)

E-mail: vaspir@cicese.mx

P.L. Swart and A.A. Chtcherbakov (EE Dept., Faculty of Engineering, Rand Afrikaans University, PO Box 524, Auckland Park 2006, Republic of South Africa)

References

1 DAKIN, J.P.: 'Distributed optical fiber sensors' in UDD, E. (Ed.): 'Fiber optic smart structures' (John Wiley & Sons, New York, 1995)
2 SPIRIN, V.V., SHLYAGIN, M.G., MIRIDONOV, S.V., and SWART, P.L.: 'Transmission/reflection analysis for distributed optical fibre loss sensor interrogation', Electron. Lett., 2002, 38, pp. 117–118
3 SPIRIN, V.V., SHLYAGIN, M.G., MIRIDONOV, S.V., and SWART, P.L.: 'Alarm-condition detection and localization using Rayleigh scattering for a fiber optic bending sensor with an unmodulated light source', Opt. Commun., 2002, 205, pp. 37 41
4 SPIRIN, V.V.: 'Transmission-reflection analysis for localization of temporally successive multi-point perturbations in distributed fiber-optic loss sensor based on Rayleigh backscattering', Appl. Opt., 2003, 42, pp. 1 7

Effect of coating heating by high power in optical fibres at small bend diameters

S.L. Logunov and M.E. DeRosa

The heating effect in highly bent singlemode optical fibres under high power conditions was studied. It was found that heating of the coating depends on the bend radius and the type of telecommunication fibre used. The detected heating only occurred at bend diameters much smaller than that recommended for normal deployment.

Introduction: Recent developments in optical networks using powerful optical amplifiers have brought the average level of optical power in singlemode optical fibres for certain applications close to 1–2 W. At such high power levels the effect of optical power on the lifetime of the optical fibre becomes more of a concern.

There are several studies that have investigated high continuous-wave (CW) power damage in optical fibre. One such phenomenon is called the fibre fuse [1] in which fibres burn back under high power exposure. Another more recent study reported the catastrophic effects high power could induce in bent optical fibre of very small bend diameter [2].

We examined the heating effect high power has on the fibre coating due to leaking of the guiding mode into the coating of fibres under high bend conditions. The coating, due to its significant overtone absorption bands in the telecommunication wavelength window of 1300–1650 nm, absorbs the cladding modes and heats the coating at the bend location. The composition of the coating and index profile of the fibres are key characteristics of the heating mechanism. Our aim in this Letter is to report the magnitude of the heating in the coating against laser power, type of fibre, coating properties, and degree of bend.

Experiment: We used two different low-loss transmission singlemode fibre types with various index profiles coated with primary and secondary layers of acrylate polymer materials. The first fibre type is characterised as standard singlemode having a step index profile with a 0.35% index Delta ($\Delta n/n$), a core diameter of 8.7 μm and a modefield diameter of 10.5 μm at 1550 nm. The second fibre type we examined is characterised as having a segmented core index profile, and a modefield diameter of 9.7 μm at 1550 nm. We also examined a

hermetically coated step index fibre which comprised a dual layer acrylate coating and a 500 Å layer of graphite on the surface of the glass cladding. All fibres were singlemode at wavelengths utilised in the study.

The test fibres of approximately 10 m in length were setup in a thermal isolation holder and bent to a single loop with diameters from 12 -25 mm. All bend diameters examined were smaller than that recommended for normal operation. The temperature rise in the coating of the fibre was monitored with a calibrated thermal heat imaging camera with a sensitivity of ~1 C.

Two high power fibre lasers were used for our tests: an erbium fibre laser at 1550 nm (IPG Photonics) and a Raman laser at 1480 nm (Spectra Physics). We increased the power from a few mW up to 2 W and monitored the temperature in the fibre coating against fibre bend diameter, input power, and wavelength. Fibre loops were tested while the bend region was not in contact with any material. We also tested fibres on a steel mandrel, which was used as a heatsink to reduce the temperature rise.

Results and discussion: A typical near infrared (NIR) spectrum of the polymer shows significant vibrational overtone absorption bands of C–H, O–H, and N–H dominating in the 1200–1650 nm wavelength region [3]. These vibrational modes absorb the power that is leaked into the cladding in the bend region and cause the coating to heat up. The temperature rise is linear with power increase according to a simple thermal analysis developed earlier for straight propagation of radiation [4]

$$\Delta T \sim \frac{\alpha(\lambda)P}{4\pi K} \tag{1}$$

where T is temperature, K is thermal conductivity, P is optical power, and $\alpha(\lambda)$ is absorption of the polymer at given wavelength λ.

Since the resulting heating is a linear function of the applied power, the temperature rise in the coating can be represented as a photothermal heating coefficient (Ht) in units C/mW of input power. This parameter is a function of bend diameter, wavelength, and index profile of the fibre. It has a maximum value that occurs when all the power in the fibre is deposited in the coating at the smallest possible area. Fig. 1 shows the wavelength dependence of the temperature rise in the segmented core index profile fibre, which is linear against bend loss. The difference found in photothermal behaviour between 1480 and 1550 nm can be readily explained using (1). Ht relates directly to the absorption coefficient of the polymer coating materials and is higher at 1480 than at 1550 nm. Typically in optical fibres, both primary and secondary coatings are used and the heating is an average result for the two coatings.
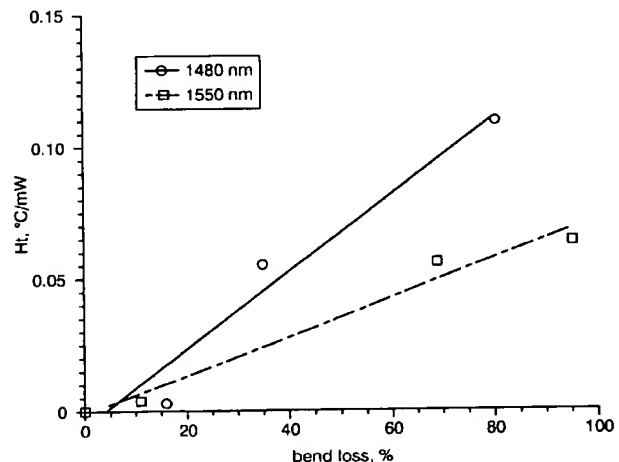

Fig. 1 Photothermal coefficient against per cent bend loss for segmented core index profile fibre at 1550 and 1480 nm

To illustrate the absorption effect in the coating even further, we exposed a transmission fibre with a carbon hermetic coating. In this case the thermal heating was the largest among all studied fibres, as shown in Fig. 2. This is so because the carbon has a much higher